Journal of Zhejiang University-SCIENCE B (Biomedicine & Biotechnology) 2023 24(5):406-417
www.jzus.zju.edu.cn; www.springer.com/journal/11585
E-mail: jzus_b@zju.edu.cn

Research Article

https://doi.org/10.1631/jzus.B2200694

Role of selenoprotein M knockdown in the melatonin antagonism of nickel-induced apoptosis and endoplasmic reticulum stress in mouse heart

Xintong ZHANG[1*], Xiaoxue GAI[2*], Lihua XU[1], Wenxue MA[1], Qiaohan LIU[1], Bendong SHI[1], Cheng FANG[1], Jingzeng CAI[1✉], Ziwei ZHANG[1,3✉]

[1]*College of Veterinary Medicine, Northeast Agricultural University, Harbin 150030, China*
[2]*Suihua Agricultural and Rural Bureau, Suihua 152000, China*
[3]*Key Laboratory of the Provincial Education, Department of Heilongjiang for Common Animal Disease Prevention and Treatment, Northeast Agricultural University, Harbin 150030, China*

Abstract: The aim of this study was to investigate the role of selenoprotein M (SelM) in endoplasmic reticulum stress and apoptosis in nickel-exposed mouse hearts and to explore the detoxifying effects of melatonin. At 21 d after intraperitoneal injection of nickel chloride ($NiCl_2$) and/or melatonin into male wild-type (WT) and SelM knockout (KO) C57BL/6J mice, $NiCl_2$ was found to induce changes in the microstructure and ultrastructure of the hearts of both WT and SelM KO mice, which were caused by oxidative stress, endoplasmic reticulum stress, and apoptosis, as evidenced by decreases in malondialdehyde (MDA) content and total antioxidant capacity (T-AOC) activity. Changes in the messenger RNA (mRNA) and protein expression of genes related to endoplasmic reticulum stress (activating transcription factor 4 (ATF4), inositol-requiring protein 1 (IRE1), c-Jun N-terminal kinase (JNK), and C/EBP homologous protein (CHOP)) and apoptosis (B-cell lymphoma-2 (Bcl-2), Bcl-2-associated X protein (Bax), Caspase-3, Caspase-9, and Caspase-12) were also observed. Notably, the observed damage was worse in SelM KO mice. Furthermore, melatonin alleviated the heart injury caused by $NiCl_2$ in WT mice but could not exert a good protective effect in the heart of SelM KO mice. Overall, the findings suggested that the antioxidant capacity of SelM, as well as its modulation of endoplasmic reticulum stress and apoptosis, plays important roles in nickel-induced heart injury.

Key words: Selenoprotein M (SelM); Nickel chloride ($NiCl_2$); Melatonin; Apoptosis; Mouse heart

1 Introduction

Nickel, as a transition metal, is a product of industrial, liquid, and solid fuel use, which has been widely distributed in the environment including the air, water, and soil (Cameron et al., 2011). Exposure to nickel can cause cardiovascular and kidney diseases, lung fibrosis, lung cancer, and nasal cancer in humans (Genchi et al., 2020). Clinical cases have shown that drinking water contaminated with nickel chloride ($NiCl_2$) causes shortness of breath and dizziness, and the accidental consumption of nickel sulfate ($NiSO_4$) can result in cardiac arrest and death. Animal experiments have indicated changes in the heart mass of rats after exposure to $NiCl_2$ (Das et al., 2018). In terms of mechanisms of action, the generation of reactive oxygen species (ROS) was thought to be involved in the underlying mechanism of heavy metal-induced toxicity (Rehman et al., 2018). Previous studies have confirmed that nickel sulfide increases ROS formation in rat lymphocytes in a concentration-dependent manner (Chakrabarti and Bai, 1999; Zhao et al., 2021). Nickel induces apoptosis in the kidney, liver, as well as the nervous and immune systems by regulating ROS, mitochondria, and the endoplasmic reticulum (Guo et al., 2016; Liu JB et al., 2022). In addition, previous research has shown that nuclear factor of activated T cells (NFAT), nuclear factor-κB (NF-κB), activator

✉ Ziwei ZHANG, zhangziwei@neau.edu.cn
Jingzeng CAI, caijingzeng@neau.edu.cn
* The two authors contributed equally to this work
Ziwei ZHANG, https://orcid.org/0000-0002-5705-4611
Jingzeng CAI, https://orcid.org/0000-0001-6929-5431

Received Dec. 29, 2022; Revision accepted Jan. 27, 2023; Crosschecked Mar. 31, 2023

protein-1 (AP-1), and other transcription factors were activated after exposure to nickel, and triggered the increased expression of inflammatory factors, including tumor necrosis factor-α (TNF-α) and cyclooxygenase-2 (COX-2), thereby causing lung inflammation, eventually leading to lung cancer (Lu et al., 2014).

Selenoprotein M (SelM), located in the endoplasmic reticulum and containing a redox group CXXU, has attracted great interest since its discovery in 2002. Because of this unique motif, SelM can bind toxic metal ions, such as Zn^{2+}, Cd^{2+}, Hg^{2+}, and Cu^{2+}, to maintain a dynamic balance of metal ions in the organism and antagonize the damage caused by toxic metal ions (Pitts and Hoffmann, 2018). In our preliminary study, it was demonstrated that SelM was significantly downregulated in the liver of high-fat diet mice; furthermore, levels of steatosis, inflammation, oxidative stress, and fibrosis were higher in the liver of SelM knockdown mice fed with a high-fat diet (Cai et al., 2022). SelM overexpression caused a significant rise in extracellular signal-regulated protein kinase (ERK) phosphorylation in the brain, heart, liver, and intestine, so as to promote the regulation of various functions (Lee et al., 2009).

Melatonin (*N*-acetyl-5-methoxytryptamine, MT) is a hormone produced by the pineal gland and other tissues. It is involved in physiological processes, including sleep promotion, circadian regulation, immune regulation, and thermoregulation, which has also been investigated for its anti-microbial, anti-cancer, and anti-inflammatory properties, as well as its potential benefits for neurodegenerative, periodontal, and cerebrovascular diseases (Roohbakhsh et al., 2018). MT relieved 2,2,4,4-tetra-brominated diphenyl ether (PBDE-47)-induced necroptosis and the secretion of inflammatory factors through the miR-140-5p/Toll-like receptor 4 (TLR4)/NF-κB axis (Li XY et al., 2022). Previous experiments have shown that MT has a significant protective effect against ischemia/reperfusion (I/R) injury, atherosclerosis, and hypertension (Roohbakhsh et al., 2018). Moreover, it was demonstrated that MT prevented ultraviolet (UV)-induced skin damage caused by ROS, apoptosis, and mitochondrial dysfunction (Kleszczyński et al., 2011; Wang CX et al., 2021). According to a growing body of literature, MT may exert its antioxidant effects by modulating the endoplasmic endoplasmic reticulum stress response (Fernandez et al., 2015).

In this study, we established a SelM knockout (KO) mice model to evaluate nickel-induced myocardial injury, analyze the role of SelM in this model, and assess the alleviating impact of MT.

2 Materials and methods

2.1 Grouping of test animals and sample collection

Male wild-type (WT) and SelM KO C57BL/6J mice were purchased from Cyagen Biosciences (Cyagen Inc., USA). A total of 80 mice, both WT and SelM KO, were divided into eight groups, including WT control group (control), WT+$NiCl_2$ group (Ni), WT+MT group (MT), WT+$NiCl_2$+MT group (Ni+MT), KO control group (KO control), KO+$NiCl_2$ group (KO Ni), KO+MT group (KO MT), and KO+$NiCl_2$+MT group (KO Ni+MT), with ten mice per group.

The mice were gavaged with 2 mg/kg MT (MedChemExpress, USA) at 9:00 a.m. and 10 mg/kg $NiCl_2$ (Sigma, St. Louis, MO, USA) at 5:00 p.m. daily; the control group was treated with saline. Modeling was euthanized for 21 d. Each mouse had free access to water and food during the test. The mice were euthanized on Day 22, and the hearts were quickly removed after soaking in alcohol. A portion of the heart tissue was placed in 4% (volume fraction) paraformaldehyde solution for hematoxylin and eosin (H&E) staining, another portion was stored at 4 ℃ in 2.5% (volume fraction) glutaraldehyde solution for transmission electron microscopy (TEM), a third portion was used for kit assays, and the remaining heart tissue was stored at −80 °C for later messenger RNA (mRNA) and protein measurements.

2.2 H&E staining

The microstructure of the heart was evaluated by H&E staining. Hearts fixed in 4% paraformaldehyde were removed, sequentially dehydrated in a series of 75%, 85%, 90%, and 95% (volume fraction) alcohol, followed by embedding and deparaffinization (Zheng et al., 2021). After H&E staining, sections were sequentially placed in an ascending alcohol gradient for dehydration. Next, sections were placed in xylene and finally sealed with neutral resin. Observation and image acquisition were performed under a microscope at 2000× magnification (Olympus Corporation, IX53, Japan).

2.3 TEM

A transmission electron microscope (HITACHI, Japan) was used to examine the heart tissue. In brief, samples were removed from a solution containing 2.5% glutaraldehyde (Merck KGaA, Darmstadt, Germany), washed with phosphate-buffered saline (PBS), fixed for 90 min in a solution containing 1% (volume fraction) tetraoxomic acid (Aladdin, Shanghai, China), dehydrated with various concentrations of ethanol (Shandong Lierkang Disinfection Technology Co., Ltd., China), and then replaced with acetone. Finally, resin was employed for embedding and the tissue was cut into sections of 50–60 nm thickness (Liu Q et al., 2022a) by employing lead citrate and uranyl acetate for double-staining experiments. TEM at a magnification of 20 000× was performed to examine the ultrastructure (Miao et al., 2022b).

2.4 Malondialdehyde kit and total antioxidant capacity kit

Malondialdehyde (MDA) kit (A003-1-2, Nanjing Jiancheng Bioengineering Institute, Nanjing, China) and total antioxidant capacity (T-AOC) kit (A015-1-2, Nanjing Jiancheng Bioengineering Institute) were used to determine the antioxidant capacity of the heart. The mouse heart tissue was ground into a homogenate and processed according to the kit instructions (Song et al., 2021). MDA kit: firstly, the homogenate and reagents were added to centrifuge tubes in sequence and mixed, then heated in warm water at 95 °C for 40 min, cooled, and centrifuged at 3500 r/min for 10 min; finally, the absorbance of the solutions in each tube was determined at 532 nm. T-AOC kit: after mixing heart tissue homogenate and reagents, the solution was left for 10 min, and the absorbance values were determined at 520 nm.

2.5 RNA isolation and quantitative real-time PCR analysis

Total RNA was separated from lymphocytes in both the control and $NiCl_2$ treatment groups by TRIzol reagent at 18 h. Complementary DNA (cDNA) was synthesized according to the instructions provided with a reverse transcription kit (Transgene, Beijing, China). Apoptosis-specific primers (B-cell lymphoma-2 (Bcl-2), Bcl-2-associated X protein (Bax), Caspase-3, Caspase-9, and Caspase-12) and endoplasmic reticulum stress-specific primers (glucose-regulated protein 94 (GRP94), GRP78, C/EBP homologous protein (CHOP), c-Jun N-terminal kinase (JNK), protein kinase RNA-like endoplasmic reticulum kinase (PERK), activating transcription factor 4 (ATF4), ATF6, X-box-binding protein 1 (XBP1), inositol-requiring enzyme 1 (IRE1)) (Table 1) were designed based on known primer sequences using Primer BLAST at the National Center for Biotechnology Information (NCBI) (Gong et al., 2022). Quantitative real-time polymerase chain reaction (qPCR) was performed using a BIOER detection system (Hangzhou, China). All reactions were performed in a 10-μL reaction mixture containing 5 μL of 2× SYBR Green I PCR MasterMix (BIOER Technology, Hangzhou, China), 1 μL of cDNA, 0.3 μL of each primer (10 μmol/L), and 3.4 μL of PCR grade water (Li JH et al., 2022). The relative abundance of each mRNA was calculated according to the $2^{-\Delta\Delta C_T}$ method, and values were normalized to the mean expression of glyceraldehyde-3-phosphate dehydrogenase (GAPDH) (Liu XJ et al., 2022; Cao et al., 2023).

2.6 Protein extraction and western blot analysis

Each group of hearts was collected, lysed on ice with radio immunoprecipitation assay (RIPA) buffer and phenylmethylsulfonyl fluoride (PMSF), and then centrifuged at 12 000 r/min and 4 °C for 25 min. Sodium dodecyl sulfate (SDS) was added to the supernatant, and samples were boiled for 10 min and preserved at −20 °C for detection (Chen et al., 2021). Proteins were isolated and transferred to nitrocellulose membranes after SDS-polyacrylamide gel electrophoresis (PAGE). Next, immunoblotting was performed, and membranes were blocked with 5% (0.05 g/mL) skimmed milk at 37 °C for 2 h and then incubated with primary antibodies overnight. The protein expression of apoptosis-specific primers (Bax, Bcl-2, Caspase-3, Caspase-9, and Caspase-12) and endoplasmic reticulum stress-specific primers (ATF6, ATF4, CHOP, IRE1, JNK, and GRP78) was detected. The dilution ratios of primary antibodies are shown in Table 2. Subsequently, membranes were washed three times with 1× PBS-Tween-20 (PBST), incubated with a secondary antibody at room temperature for 1 h, and washed three times with 1× Tris-buffered saline-Tween-20 (TBST) (Zhang WY et al., 2023). The protein bands were visualized using enhanced chemiluminescence detection reagents (Applygen Technologies

Inc., Beijing, China) and X-ray films (TransGen Biotech Co., Beijing, China). The relative abundance of proteins was standardized using β-actin as control (Qiao et al., 2022; Zhang YH et al., 2023).

2.7 Data analysis

Statistical analysis was carried out by one-way analysis of variance (ANOVA) using GraphPad Prism Version 8.0 software, and Tukey's multiple comparison test was conducted to analyze the differences (Liu Q et al., 2022b; Zhang et al., 2022). All experiments were performed at least six times. The results were expressed as mean±standard deviation (SD). Significant differences between two or more groups were indicated by $P<0.05$; in case no significant differences between different groups were observed, $P>0.05$.

3 Results

3.1 Microscopic observation of the heart

Fig. 1 shows that the microstructures of mouse cardiomyocytes in the control and KO control group

Table 1 Primers used in the present study

Gene name	Forward (5'→3')	Reverse (5'→3')
GRP94	CTTCTACCAGACACCAAGGCGTATG	GTTCTTCCTCCACCTGTGCTTCAG
GRP78	ATGATGAAGTTCACTGTGGTGG	CTGATCGTTGGCTATGATCTCC
PERK	GAGATCTGGCTCAAAGACGAAA	AAGGAGCTATGACTTCGATCTG
ATF4	AGTTTAGAGCTAGGCAGTGAAG	CATACAGATGCCACTGTCATTG
IRE1	TTACACATAGTACACCGTGACC	CAGAATGGAGACTGAAGCTACA
XBP1	TTGCCTCTTCAGATTCTGAGTC	CCAGGTGATGCCTTTGTTCTTGTTG
Cyt c	CCAAATCTCCACGGTCTGTTCGG	AAGGAGCTATGACTTCGATCTG
Bax	AGGCCTCCTCTCCTACTTCG	CCTTTCCCCTTCCCCCATTC
Bcl-2	AGCATGCGACCTCTGTTTGA	GCCACACGTTTCTTGGCAAT
Caspase-3	GAAACTCTTCATCATTCAGGCC	GCGAGTGAGAATGTGCATAAAT
Caspase-9	TGTGAATATCTTCAACGGGAGC	GAGTAGGACACAAGGATGTCAC
Caspase-12	TGGCCCATGAATCACATCTAAT	TGGACAAAGCTTCAGTGTATCT
JNK	CGCCTTATGTGGTGACTCGCTAC	CTCCCATGATGCACCCAACTGAC
CHOP	CTCCAGATTCCAGTCAGAGTTC	ACTCTGTTTCCGTTTCCTAGTT
ATF6	TGCCTTGGGAGTCAGACCTATGG	CTGTGGACCGAGGAGAGGAGATG
GAPDH	GGCAAATTCAACGGCACAGTCAAG	TCGCTCCTGGAAGATGGTGATGG

GRP: glucose-regulated protein; PERK: protein kinase RNA-like endoplasmic reticulum kinase; ATF: activating transcription factor; IRE1: inositol-requiring enzyme 1; XBP1: X-box-binding protein 1; Cyt *c*: cytochrome *c*; Bcl-2: B-cell lymphoma-2; Bax: Bcl-2-associated X protein; JNK: c-Jun N-terminal kinase; CHOP: C/EBP homologous protein; GAPDH: glyceraldehyde-3-phosphate dehydrogenase.

Table 2 Antibodies used in the present study

Antibody name	Dilution ratio*	Size (kDa)	Company information
ATF6	1:2000	75	Proteintech, Wuhan, China
ATF4	1:1500	39	Cell Signaling Technology, Inc., Boston, USA
CHOP	1:750	19	Wanlei, Shenyang, China
IRE1	1:1500	110	ABclonal, Wuhan, China
Caspase-3	1:500	32	Proteintech, Wuhan, China
Caspase-9	1:500	42	Proteintech, Wuhan, China
Caspase-12	1:500	42	Proteintech, Wuhan, China
JNK	1:500	46	Abmart, Shanghai, China
Bax	1:1000	23	Abmart, Shanghai, China
GRP78	1:1500	78	Proteintech, Wuhan, China
Bcl-2	1:500	26	Proteintech, Wuhan, China
GAPDH	1:10 000	37	Proteintech, Wuhan, China

* Volume ratio. ATF: activating transcription factor; CHOP: C/EBP homologous protein; IRE1: inositol-requiring enzyme 1; JNK: c-Jun N-terminal kinase; Bcl-2: B-cell lymphoma-2; Bax: Bcl-2-associated X protein; GRP78: glucose-regulated protein 78; GAPDH: glyceraldehyde-3-phosphate dehydrogenase.

were neatly shaped, the myocardial fibers were evenly aligned, and staining was uniform. In contrast, mice in the Ni group had more disorganized myocardial fibers with wavy bending, crumpling, and even lysis. In addition, gaps and inflammatory cell infiltration were visible between cells, and myocardial fibers in the KO Ni group were significantly disorganized with increased gaps.

3.2 Ultrastructural observation of the heart

TEM was employed to evaluate the ultrastructure of mouse heart tissue, and the results are shown in Fig. 2. The nuclei of mouse heart tissue of the control group were intact and a large number of clear mitochondria were visible. Meanwhile, mice in the Ni group exhibited nuclear wrinkling, mitochondrial enlargement, and loss of mitochondrial cristae. Cardiomyocyte nuclei in the KO Ni group were more wrinkled compared to the Ni group, and the endoplasmic reticulum and mitochondria were fragmented.

3.3 Determination of heart antioxidant capacity

The antioxidant capacity of the mouse heart was assessed by measuring the MDA content and T-AOC activity. The results are depicted in Fig. 3. The activity of T-AOC in the mouse heart of the Ni group was significantly reduced compared to the control group (P<0.05), while the content of MDA was significantly

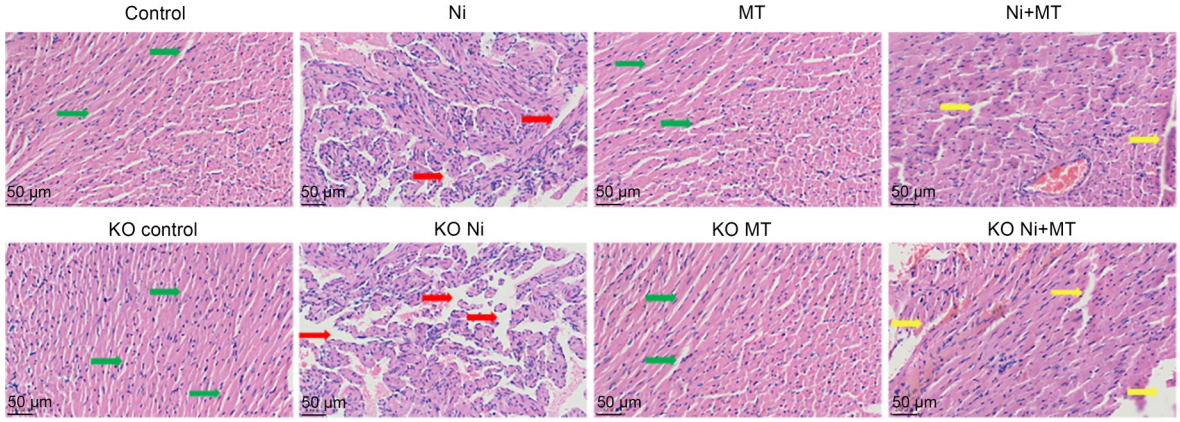

Fig. 1 Results of H&E staining of the hearts of WT and SelM KO mice after exposure to $NiCl_2$ and/or MT. Control: WT control group; Ni: WT+$NiCl_2$ group; MT: WT+MT group; Ni+MT: WT+$NiCl_2$+MT group; KO control: KO control group; KO Ni: KO+$NiCl_2$ group; KO MT: KO+MT group; KO Ni+MT: KO+$NiCl_2$+MT group. The green arrows indicate the normal morphology of myocardial fibers; the red arrows indicate widely spaced myocardial fibers; the yellow arrows indicate abnormal myocardial fiber distances. H&E: hematoxylin and eosin; WT: wild-type; SelM: selenoprotein M; KO: knockout; $NiCl_2$: nickel chloride; MT: melatonin.

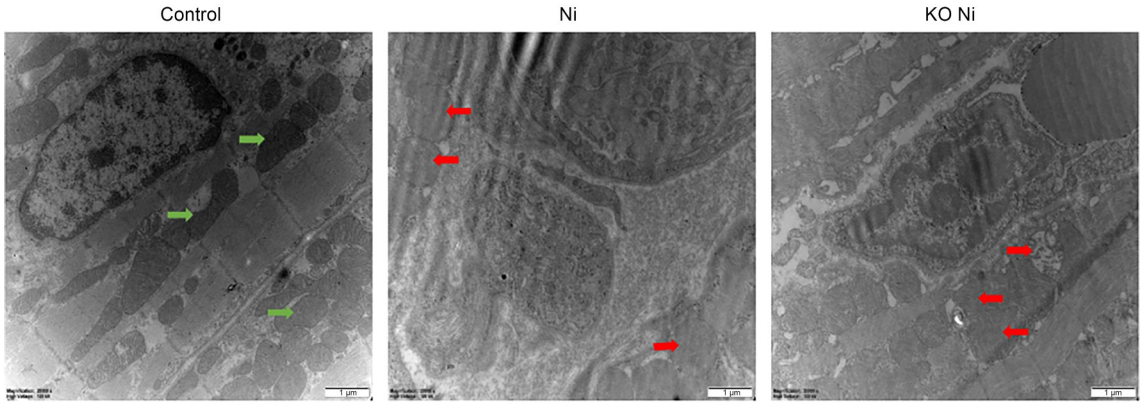

Fig. 2 TEM results of cardiac ultrastructure in WT and SelM KO mice after exposure to $NiCl_2$. Control: WT control group; Ni: WT+$NiCl_2$ group; KO Ni: KO+$NiCl_2$ group. The green arrows indicate normal mitochondrial morphology; the red arrows indicate abnormal mitochondria or endoplasmic reticulum. TEM: transmission electron microscopy; SelM: selenoprotein M; WT: wild-type; KO: knockout; $NiCl_2$: nickel chloride.

increased (P<0.05). However, after MT treatment, the cardiac MDA content and T-AOC activity were reversed (P<0.05), which was also the case in KO mice. It should be noted that the MDA content of the Ni group was significantly lower than that of the KO Ni group (P<0.05).

3.4 mRNA and protein expression of endoplasmic reticulum stress-associated genes

The protective effect of MT against nickel-induced endoplasmic reticulum stress was investigated using mRNA and protein expression assays on cardiac tissues (Fig. 4). The PCR results showed that Ni significantly increased the mRNA expression of *GRP94*, *IRE1*, *CHOP*, *ATF4*, *XBP1*, *PERK*, and *JNK* (P<0.05), while the mRNA expression of *GRP78* or *ATF6* was not significant (P>0.05). The results of western blot analysis showed that the protein expression of ATF4, ATF6, IRE1, GRP78, CHOP, and JNK was significantly higher in the Ni group compared to the control group (P<0.05). The protein expression was significantly lower in the Ni+MT group compared with the Ni group (P<0.05). Notably, except for GRP78, the mRNA and protein levels were significantly increased in KO Ni mice compared with the Ni group (P<0.05).

3.5 mRNA and protein expression of apoptosis-related genes

Fig. 5a presents the effects of $NiCl_2$ exposure on the mRNA expression levels of apoptotic genes *Bax*, *Bcl-2*, cytochrome *c* (*Cyt c*), *Caspase-3*, *Caspase-9*, and *Caspase-12* in mouse hearts. The PCR results revealed that the mRNA expression of *Bax*, *Cyt c*, *Caspase-3*, *Caspase-9*, and *Caspase-12* was increased (P<0.05) in the Ni group, while the mRNA expression of *Bcl-2* was decreased (P<0.05). These findings were alleviated by treatment with MT. Fig. 5b shows the protein results of apoptosis-related genes by western blot analysis. In the Ni group, the protein expression of Bax, Caspase-3, Caspase-9, and Caspase-12 increased while Bcl-2 expression decreased (P< 0.05). Furthermore, MT significantly reduced the Ni-induced increase in apoptosis genes (P<0.05). Notably, when compared to the Ni group, levels of apoptosis-related mRNAs and proteins were significantly increased in the KO Ni group (P<0.05), whereas Bcl-2 expression was significantly decreased (P<0.05). Taken together, these findings indicated that apoptotic damage was more severe in SelM KO mice compared to WT mice, and Ni-induced apoptosis was alleviated by MT.

Fig. 6a shows the correlation of expression of different genes determined in mouse hearts: apoptosis-related genes positively correlated with endoplasmic reticulum stress-related genes, except for Bcl-2. The protein–protein interaction (PPI) network (Fig. 6b) shows gene interactions; the interacting genes included *ATF4*, *ATF6*, *Caspase-3*, *Caspase-9*, *Bax*, *Bcl-2*, and *XBP1*, suggesting that these genes play key roles in the MT antagonism of nickel-induced apoptosis and endoplasmic reticulum stress, in which SelM is involved.

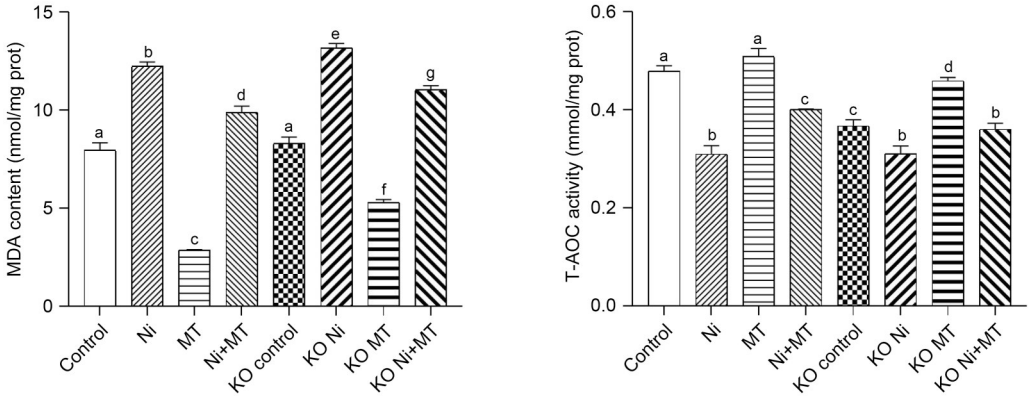

Fig. 3 MDA content and T-AOC activity of the mouse heart. Control: WT control group; Ni: WT+$NiCl_2$ group; MT: WT+MT group; Ni+MT: WT+$NiCl_2$+MT group; KO control: KO control group; KO Ni: KO+$NiCl_2$ group; KO MT: KO+MT group; KO Ni+MT: KO+$NiCl_2$+MT group. Data are expressed as mean±SD (n=6). Different letters indicate statistical differences between the different groups (P<0.05); in case of no differences, the same letters are used. MDA: malondialdehyde; T-AOC: total antioxidant capacity; WT: wild-type; KO: knockout; MT: melatonin; SD: standard deviation; prot: protein.

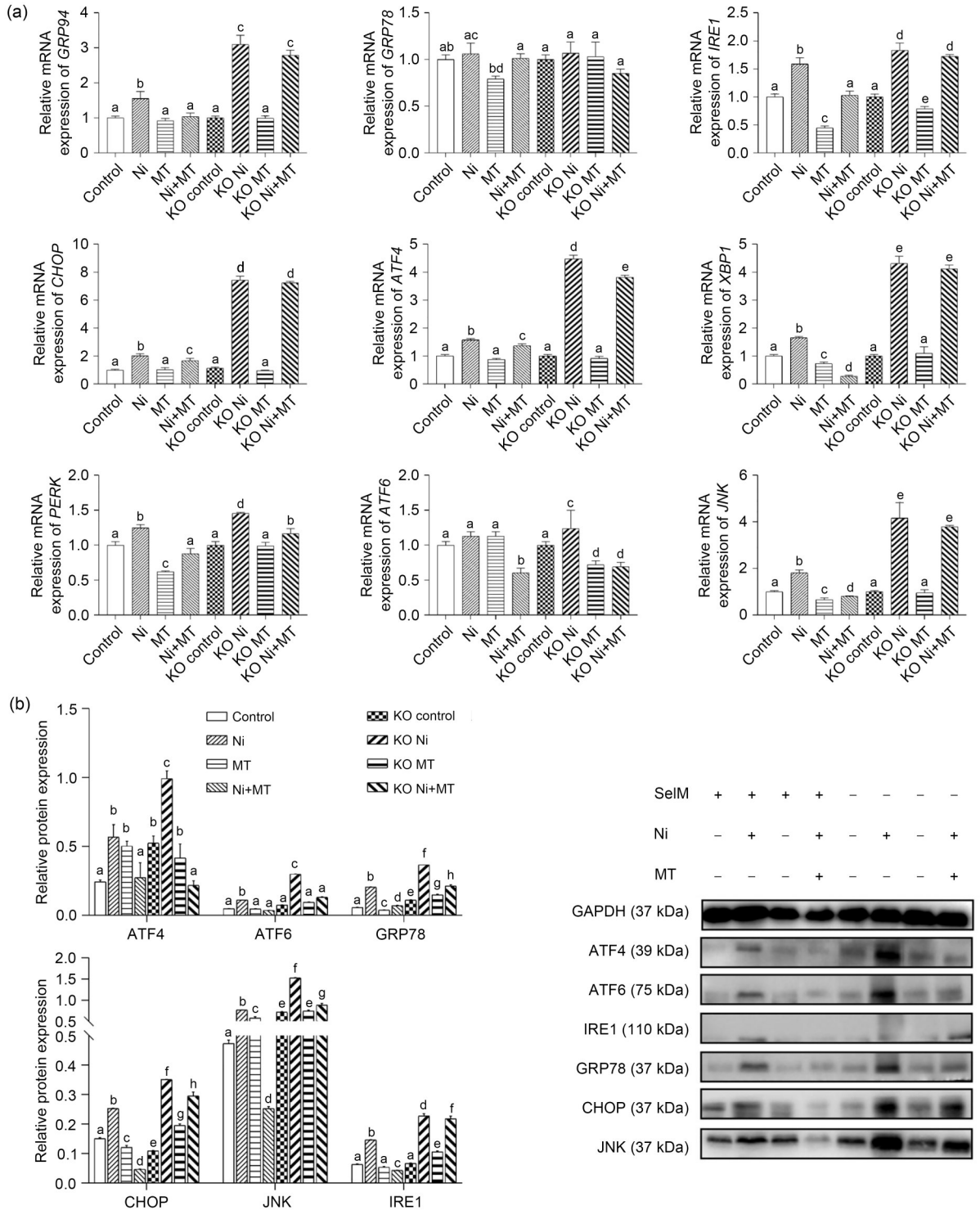

Fig. 4 mRNA (a) and protein (b) expression results of endoplasmic reticulum stress-related genes. Control: WT control group; Ni: WT+$NiCl_2$ group; MT: WT+MT group; Ni+MT: WT+$NiCl_2$+MT group; KO control: KO control group; KO Ni: KO+$NiCl_2$ group; KO MT: KO+MT group; KO Ni+MT: KO+$NiCl_2$+MT group. Data are expressed as mean±SD (*n*= 6). Different letters indicate statistical differences between the different groups (*P*<0.05); in case of no differences, the same letters are used. mRNA: messenger RNA; WT: wild-type; KO: knockout; MT: melatonin; GRP: glucose-regulated protein; IRE1: inositol-requiring enzyme 1; CHOP: C/EBP homologous protein; ATF: activating transcription factor; XBP1: X-box-binding protein 1; PERK: protein kinase RNA-like endoplasmic reticulum kinase; JNK: c-Jun N-terminal kinase; GAPDH: glyceraldehyde-3-phosphate dehydrogenase; SD: standard deviation.

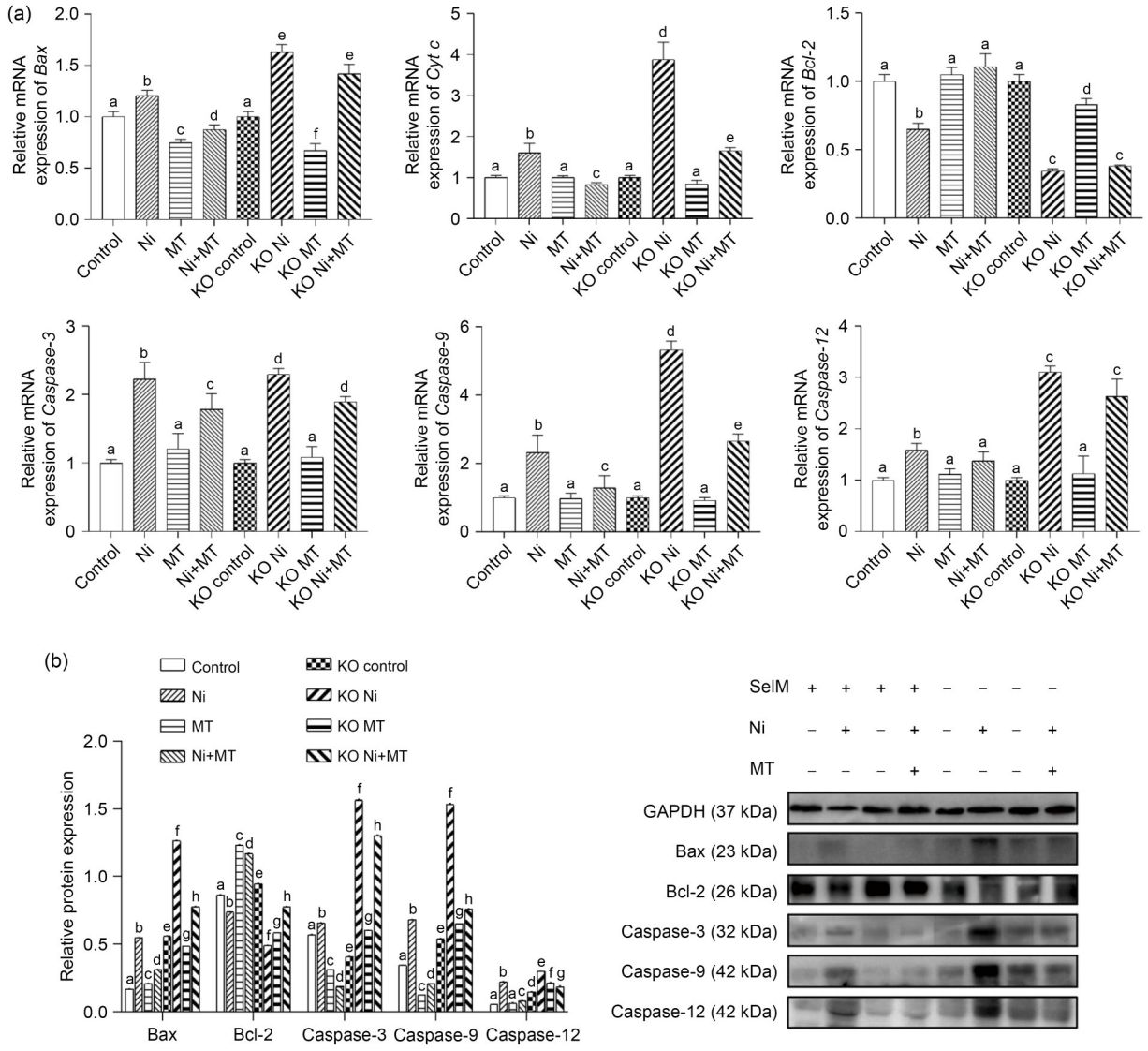

Fig. 5 mRNA (a) and protein (b) expression results of apoptosis-related genes. Control: WT control group; Ni: WT+$NiCl_2$ group; MT: WT+MT group; Ni+MT: WT+$NiCl_2$+MT group; KO control: KO control group; KO Ni: KO+$NiCl_2$ group; KO MT: KO+MT group; KO Ni+MT: KO+$NiCl_2$+MT group. Data are expressed as mean±SD (n=6). Different letters indicate statistical differences between the different groups (P<0.05); in case of no differences, the same letters are used. mRNA: messenger RNA; WT: wild-type; KO: knockout; MT: melatonin; Bcl-2: B-cell lymphoma-2; Bax: Bcl-2-associated X protein; Cyt *c*: cytochrome *c*; GAPDH: glyceraldehyde-3-phosphate dehydrogenase; SD: standard deviation.

4 Discussion

Previous studies have highlighted that Sec-to-Cys mutant selenoprotein M (SelM') is capable of binding and modulating Zn^{2+}-mediated ROS production and neurotoxicity. That is, SelM may be involved in regulating the redox balance as well as metal homeostasis (Du et al., 2013). It has previously been observed that costimulation of SelM overexpression and selenium treatment may modulate multiple functions in the heart by inducing a significant change in ERK phosphorylation (Lee et al., 2009; Miao et al., 2022a). In addition, recent work has demonstrated that following nickel exposure, glutathione peroxidase (GPX) activity decreases and superoxide dismutase (SOD) activity increases in the brain and heart of goldfish (Kubrak et al., 2014). In our study, after exposure to nickel, myocardial fibers in WT mice displayed wavy bending, crinkling, and lysis phenomena, as well as a significant infiltration of inflammatory cells between

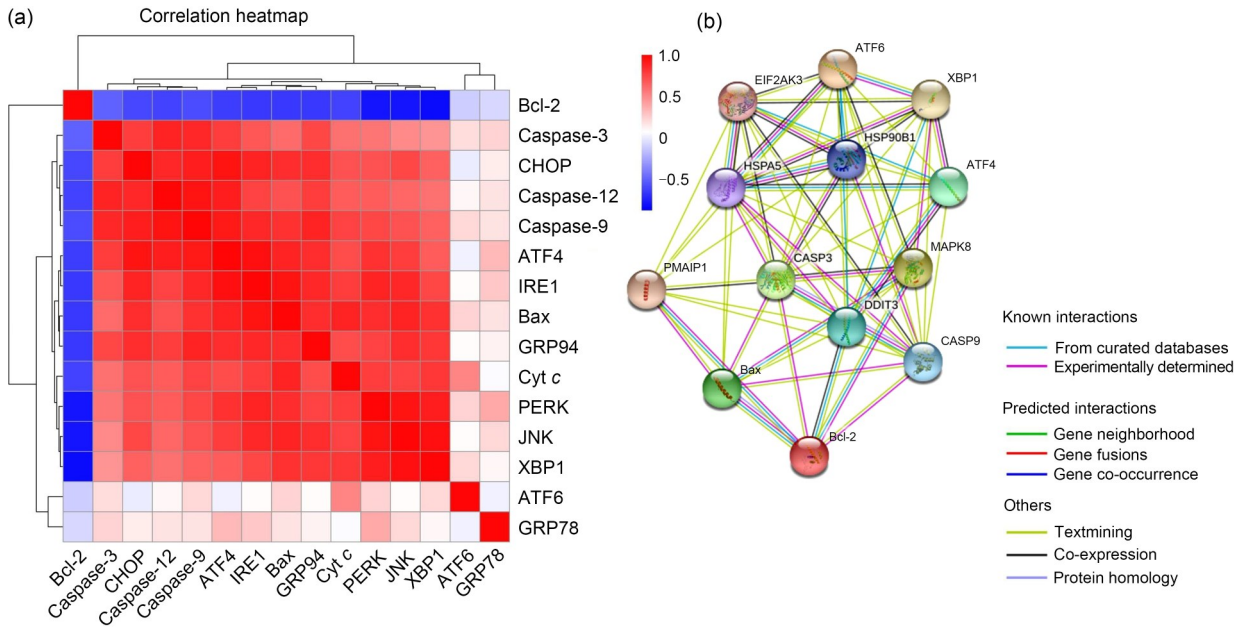

Fig. 6 Correlation of expression of apoptosis-related genes and endoplasmic reticulum stress-related genes in mouse hearts. (a) Correlation heatmap indicates the correlation of detected gene expression in mouse hearts exposed to $NiCl_2$ and/or MT, where red indicates a positive correlation and blue indicates a negative correlation. (b) PPI network was regulated between apoptosis and endoplasmic reticulum stress based on the String database in mouse hearts exposed to $NiCl_2$ and/or MT. $NiCl_2$: nickel chloride; MT: melatonin; PPI: protein–protein interaction; Bcl-2: B-cell lymphoma-2; CHOP: C/EBP homologous protein; ATF: activating transcription factor; IRE1: inositol-requiring enzyme 1; Bax: Bcl-2-associated X protein; GRP: glucose-regulated protein; Cyt *c*: cytochrome *c*; PERK: protein kinase RNA-like endoplasmic reticulum kinase; JNK: c-Jun N-terminal kinase; XBP1: X-box-binding protein 1; EIF2AK3: eukaryotic translation initiation factor 2 alpha kinase 3; HSP90B1: heat shock protein 90 kDa beta (GRP94) member 1; PMAIP1: phorbol-12-myristate-13-acetate-induced protein 1; CASP: caspase; MAPK8: mitogen-activated protein kinase 8; DDIT3: DNA damage-inducible transcript 3 (Note: for interpretation of the references to color in this figure legend, the reader is referred to the web version of this article).

cells. Myocardial fibers in SelM KO mice displayed even greater disorganization, with clear gaps and more severe damage. Ultrastructural examination revealed that the nuclei of the control group were unharmed and the mitochondria were clear. In the nickel-exposed group, the nucleus was wrinkled and the mitochondria were expanded, while the endoplasmic reticulum was ruptured in the nuclei of SelM KO mice. Overall, these findings showed that nickel severely damaged mouse cardiac tissue, and the damage was worse in SelM KO mice.

SelM is a protein containing selenocysteine, has redox activity, and is involved in antioxidant reactions (Lu et al., 2012). It was previously found that the endoplasmic reticulum stress inducer dithiothreitol (DTT) alters the expression of selenoproteins (SelS, SelK, SelT, SelM, and SelN) in MCF7 breast cancer cells (Selvik et al., 2013). In chickens with cartilage damage and selenium deficiency, miR-138-5p participated in the mitochondrial apoptosis pathway by targeting SelM in chicken chondrocytes (Chi et al., 2019). Furthermore, nano-selenium protected rat kidney cells exposed to $NiSO_4$ by inhibiting endoplasmic reticulum stress and mitochondrial pathway apoptosis (Wang Y et al., 2021). In sesamin prevention experiments against nickel-induced hepatotoxicity, $NiCl_2$ increased the levels of ROS and lipid peroxidation, decreased the activity of antioxidant enzymes (total SOD (T-SOD), catalase (CAT), and GPX), and promoted apoptosis by modulating the phosphatidylinositol 3-kinase (PI3K)-protein kinase B (Akt) signaling pathway (Liu et al., 2013; Li XJ et al., 2022). Our data showed that nickel exposure increased the mRNA and protein expression of IRE1, ATF6, ATF4, CHOP, JNK, BAX, Caspase-3, Caspase-12, and Caspase-9 in mouse heart tissue and decreased that of Bcl-2. Thus, these findings imply that too much nickel may cause stress on the endoplasmic reticulum and apoptosis in mouse hearts. Notably, the expression was more obvious in the hearts of SelM KO mice, indicating that SelM KO

influences nickel-induced apoptosis through controlling endoplasmic reticulum stress.

MT is an indole derivative produced by the pineal gland that antagonizes the toxic effects of heavy metals. Recent studies have shown that MT prevents cadmium-induced nephrotoxicity by alleviating oxidative stress, restoring the mitochondrial membrane potential, and inhibiting mitochondrial fission mediated by dynamin-related protein 1 (Drp1) and mitochondrial fission protein 1 (Fis1) (Dong et al., 2022). Lead toxicity caused neurotoxicity and oxidative stress in the rat cerebellum at specific developmental stages, whereas MT alleviated motor deficits and oxidative stress by antagonizing lead toxicity (Suresh et al., 2006; Fan et al., 2021). In this study, MT alleviated myocardial injury caused by Ni by alleviating oxidative stress and regulating the IRE1/JNK/Caspase-3 pathway. Compared with the Ni+MT group, heart injury in the KO Ni+MT group was more severe. Data obtained from mRNA and western blot analysis showed that, except for the mRNA of *GRP78*, the mRNA and protein expression of stress and apoptosis genes in the endoplasmic reticulum of the two groups of mice was statistically different. Compared with the KO Ni group, the mRNAs of endoplasmic reticulum stress-related genes (*GRP94*, *GRP78*, *IRE1*, *CHOP*, *XBP1*, and *JNK*) in the KO Ni+MT group did not show significant changes, and the same was observed for mRNAs of apoptosis-related genes (*Bax*, *Bcl-2*, *Caspase-3*, *Caspase-9*, and *Caspase-12*). Thus, while MT alleviated some of the myocardial damage caused by nickel, it did not play a sufficient antagonistic role in SelM KO mice, indicating that SelM was very important in the process of Ni-induced myocardial damage in mice.

5 Conclusions

In this study, a $NiCl_2$ intoxication model was established in WT and SelM KO mice. MT alleviated the occurrence of oxidative stress, endoplasmic reticulum stress, and apoptosis in the hearts of WT mice, but not in the hearts of SelM KO mice, indicating that the expression of SelM in the heart played a protective role.

Data availability

The data underlying this article will be shared on reasonable request to the corresponding author.

Acknowledgments

The work was supported by the Heilongjiang Provincial Natural Science Foundation for Outstanding Youth (No. YQ2021C021), China.

Author contributions

Xintong ZHANG: writing – original draft; Xiaoxue GAI: data curation; Lihua XU: software; Wenxue MA: validation; Qiaohan LIU: visualization; Bendong SHI: methodology; Cheng FANG and Jingzeng CAI: writing – review & editing; Ziwei ZHANG: funding acquisition. All authors have read and approved the final manuscript, and therefore, have full access to all the data in the study and take responsibility for the integrity and security of the data.

Compliance with ethics guidelines

Xintong ZHANG, Xiaoxue GAI, Lihua XU, Wenxue MA, Qiaohan LIU, Bendong SHI, Cheng FANG, Jingzeng CAI, and Ziwei ZHANG declare that they have no conflict of interests.

All procedures were carried out following the directive of the Council of the European Communities (No. 86/609/EEC) and approved by the Committee on Animal Management and Use of Northeast Agricultural University (No. SRM-11), China.

References

Cai JZ, Huang JQ, Yang J, et al., 2022. The protective effect of selenoprotein M on non-alcoholic fatty liver disease: the role of the AMPKα1-MFN2 pathway and Parkin mitophagy. *Cell Mol Life Sci*, 79(7):354. https://doi.org/10.1007/s00018-022-04385-0

Cameron KS, Buchner V, Tchounwou PB, 2011. Exploring the molecular mechanisms of nickel-induced genotoxicity and carcinogenicity: a literature review. *Rev Environ Health*, 26(2):81-92. https://doi.org/10.1515/reveh.2011.012

Cao JW, Xu R, Wang FH, et al., 2023. Polyethylene microplastics trigger cell apoptosis and inflammation via inducing oxidative stress and activation of the NLRP3 inflammasome in carp gills. *Fish Shellfish Immunol*, 132: 108470. https://doi.org/10.1016/j.fsi.2022.108470

Chakrabarti SK, Bai CJ, 1999. Role of oxidative stress in nickel chloride-induced cell injury in rat renal cortical slices. *Biochem Pharmacol*, 58(9):1501-1510. https://doi.org/10.1016/s0006-2952(99)00232-4

Chen Y, Jing HY, Chen MY, et al., 2021. Transcriptional profiling of exosomes derived from *Staphylococcus aureus*-infected bovine mammary epithelial cell line MAC-T by RNA-seq analysis. *Oxid Med Cell Longev*, 2021:8460355. https://doi.org/10.1155/2021/8460355

Chi QR, Luan YL, Zhang YM, et al., 2019. The regulatory effects of miR-138-5p on selenium deficiency-induced chondrocyte apoptosis are mediated by targeting SelM. *Metallomics*, 11(4):845-857. https://doi.org/10.1039/c9mt00006b

Das KK, Reddy RC, Bagoji IB, et al., 2018. Primary concept of nickel toxicity—an overview. *J Basic Clin Physiol Pharmacol*, 30(2):141-152. https://doi.org/10.1515/jbcpp-2017-0171

Dong WX, Yan LQ, Tan Y, et al., 2022. Melatonin improves mitochondrial function by preventing mitochondrial fission in cadmium-induced rat proximal tubular cell injury via SIRT1-PGC-1α pathway activation. *Ecotoxicol Environ Saf*, 242:113879. https://doi.org/10.1016/j.ecoenv.2022.113879

Du XB, Li HP, Wang Z, et al., 2013. Selenoprotein P and selenoprotein M block Zn^{2+}-mediated $A\beta^{42}$ aggregation and toxicity. *Metallomics*, 5(7):861-870. https://doi.org/10.1039/c3mt20282h

Fan RF, Tang KK, Wang ZY, et al., 2021. Persistent activation of Nrf2 promotes a vicious cycle of oxidative stress and autophagy inhibition in cadmium-induced kidney injury. *Toxicology*, 464:152999. https://doi.org/10.1016/j.tox.2021.152999

Fernandez A, Ordóñez R, Reiter RJ, et al., 2015. Melatonin and endoplasmic reticulum stress: relation to autophagy and apoptosis. *J Pineal Res*, 59(3):292-307. https://doi.org/10.1111/jpi.12264

Genchi G, Carocci A, Lauria G, et al., 2020. Nickel: human health and environmental toxicology. *Int J Environ Res Public Health*, 17(3):679. https://doi.org/10.3390/ijerph17030679

Gong ZG, Zhao Y, Wang ZY, et al., 2022. Epigenetic regulator BRD4 is involved in cadmium-induced acute kidney injury *via* contributing to lysosomal dysfunction, autophagy blockade and oxidative stress. *J Hazard Mater*, 423:127110. https://doi.org/10.1016/j.jhazmat.2021.127110

Guo HR, Chen L, Cui HM, et al., 2016. Research advances on pathways of nickel-induced apoptosis. *Int J Mol Sci*, 17(1):10. https://doi.org/10.3390/ijms17010010

Kleszczyński K, Hardkop LH, Fischer TW, 2011. Differential effects of melatonin as a broad range UV-damage preventive dermato-endocrine regulator. *Dermatoendocrinol*, 3(1):27-31. https://doi.org/10.4161/derm.3.1.14842

Kubrak OI, Poigner H, Husak VV, et al., 2014. Goldfish brain and heart are well protected from Ni^{2+}-induced oxidative stress. *Comp Biochem Physiol C Toxicol Pharmacol*, 162:43-50. https://doi.org/10.1016/j.cbpc.2014.03.011

Lee YK, Yim SY, Jung SE, et al., 2009. The costimulation of selenium treatment and selenoprotein M overexpression significantly induced the up- and down-regulation of ERK MAPK signaling pathway in various tissues. *Lab Anim Res*, 25(3):201-205.

Li JH, Zhang WY, Zhou P, et al., 2022. Selenium deficiency induced apoptosis via mitochondrial pathway caused by oxidative stress in porcine gastric tissues. *Res Vet Sci*, 144:142-148. https://doi.org/10.1016/j.rvsc.2021.10.017

Li XJ, Bai RC, Bai YC, et al., 2022. ROS-mediated PPAR/RXR inhibition contributes to acetochlor-induced apoptosis and autophagy in *Ctenopharyngodon idella* hepatic cells. *Fish Shellfish Immunol*, 128:684-694. https://doi.org/10.1016/j.fsi.2022.08.053

Li XY, Zhang HR, Qiao SQ, et al., 2022. Melatonin administration alleviates 2,2,4,4-tetra-brominated diphenyl ether (PBDE-47)-induced necroptosis and secretion of inflammatory factors via miR-140-5p/TLR4/NF-κB axis in fish kidney cells. *Fish Shellfish Immunol*, 128:228-237. https://doi.org/10.1016/j.fsi.2022.08.004

Liu CM, Zheng GH, Ming QL, et al., 2013. Sesamin protects mouse liver against nickel-induced oxidative DNA damage and apoptosis by the PI3K-Akt pathway. *J Agric Food Chem*, 61(5):1146-1154. https://doi.org/10.1021/jf304562b

Liu JB, Li ZF, Lu L, et al., 2022. Glyphosate damages blood-testis barrier via NOX1-triggered oxidative stress in rats: long-term exposure as a potential risk for male reproductive health. *Environ Int*, 159:107038. https://doi.org/10.1016/j.envint.2021.107038

Liu Q, Sun Y, Zhu Y, et al., 2022a. Melatonin relieves liver fibrosis induced by Txnrd3 knockdown and nickel exposure via IRE1/NF-κB/NLRP3 and PERK/TGF-β1 axis activation. *Life Sci*, 301:120622. https://doi.org/10.1016/j.lfs.2022.120622

Liu Q, Du PY, Zhu Y, et al., 2022b. Thioredoxin reductase 3 suppression promotes colitis and carcinogenesis via activating pyroptosis and necrosis. *Cell Mol Life Sci*, 79(2):106. https://doi.org/10.1007/s00018-022-04155-y

Liu XJ, Wang YQ, Shang SQ, et al., 2022. TMT induces apoptosis and necroptosis in mouse kidneys through oxidative stress-induced activation of the NLRP3 inflammasome. *Ecotoxicol Environ Saf*, 230:113167. https://doi.org/10.1016/j.ecoenv.2022.113167

Lu JY, Zhang M, Jin HL, et al., 2014. Advances on molecular mechanism of chronic inflammation-driven lung cancer induced by environmental carcinogens. *Prog Biochem Biophys*, 41(1):41-51. https://doi.org/10.3724/sp.J.1206.2013.00386

Lu W, Li WW, Jin XK, et al., 2012. Reproductive function of Selenoprotein M in Chinese mitten crabs (*Eriocheir sinesis*). *Peptides*, 34(1):168-176. https://doi.org/10.1016/j.peptides.2011.04.022

Miao ZR, Miao ZY, Shi X, et al., 2022a. The antagonistic effect of selenium on lead-induced apoptosis and necroptosis via P38/JNK/ERK pathway in chicken kidney. *Ecotoxicol Environ Saf*, 231:113176. https://doi.org/10.1016/j.ecoenv.2022.113176

Miao ZR, Miao ZY, Wang SC, et al., 2022b. Exposure to imidacloprid induce oxidative stress, mitochondrial dysfunction, inflammation, apoptosis and mitophagy via NF-kappaB/JNK pathway in grass carp hepatocytes. *Fish Shellfish Immunol*, 120:674-685. https://doi.org/10.1016/j.fsi.2021.12.017

Pitts MW, Hoffmann PR, 2018. Endoplasmic reticulum-resident selenoproteins as regulators of calcium signaling and homeostasis. *Cell Calcium*, 70:76-86.

https://doi.org/10.1016/j.ceca.2017.05.001

Qiao SQ, Sun Y, Jiang YY, et al., 2022. Melatonin ameliorates nickel induced autophagy in mouse brain: diminution of oxidative stress. *Toxicology*, 473:153207. https://doi.org/10.1016/j.tox.2022.153207

Rehman K, Fatima F, Waheed I, et al., 2018. Prevalence of exposure of heavy metals and their impact on health consequences. *J Cell Biochem*, 119(1):157-184. https://doi.org/10.1002/jcb.26234

Roohbakhsh A, Shamsizadeh A, Hayes AW, et al., 2018. Melatonin as an endogenous regulator of diseases: the role of autophagy. *Pharmacol Res*, 133:265-276. https://doi.org/10.1016/j.phrs.2018.01.022

Selvik LKM, Fjeldbo CS, Flatberg A, et al., 2013. The duration of gastrin treatment affects global gene expression and molecular responses involved in ER stress and anti-apoptosis. *BMC Genomics*, 14:429. https://doi.org/10.1186/1471-2164-14-429

Song N, Wang W, Wang Y, et al., 2021. Hydrogen sulfide of air induces macrophage extracellular traps to aggravate inflammatory injury via the regulation of miR-15b-5p on MAPK and insulin signals in trachea of chickens. *Sci Total Environ*, 771:145407. https://doi.org/10.1016/j.scitotenv.2021.145407

Suresh C, Dennis AO, Heinz J, et al., 2006. Melatonin protection against lead-induced changes in human neuroblastoma cell cultures. *Int J Toxicol*, 25(6):459-464. https://doi.org/10.1080/10915810600959576

Wang CX, Zhang R, Wang S, et al., 2021. Protective effects of nano-selenium on nickel-induced renal cell apoptosis in rats. *J Toxicol*, 35(3):193-197 (in Chinese). https://doi.org/10.16421/j.cnki.1002-3127.2021.03.004

Wang Y, Zhao HJ, Liu YC, et al., 2021. Environmentally relevant concentration of sulfamethoxazole-induced oxidative stress-cascaded damages in the intestine of grass carp and the therapeutic application of exogenous lycopene. *Environ Pollut*, 274:116597. https://doi.org/10.1016/j.envpol.2021.116597

Zhang HR, Zhao FQ, Gai XX, et al., 2022. Astilbin attenuates apoptosis induced by cadmium through oxidative stress in carp (*Cyprinus carpio* L.) head kidney lymphocyte. *Fish Shellfish Immunol*, 125:230-237. https://doi.org/10.1016/j.fsi.2022.05.021

Zhang WY, Sun XY, Shi X, et al., 2023. Subacute cadmium exposure induces necroptosis in swine lung via influencing Th1/Th2 balance. *Biol Trace Elem Res*, 201(1):220-228. https://doi.org/10.1007/s12011-022-03133-6

Zhang YH, Xu S, Li K, et al., 2023. TBBPA induced ROS overproduction promotes apoptosis and inflammation by inhibiting autophagy in mice lung. *Ecotoxicol Environ Saf*, 252:114607. https://doi.org/10.1016/j.ecoenv.2023.114607

Zhao HJ, Wang Y, Liu YC, et al., 2021. ROS-induced hepatotoxicity under cypermethrin: involvement of the crosstalk between Nrf2/Keap1 and NF-κB/iκB-α pathways regulated by proteasome. *Environ Sci Technol*, 55(9):6171-6183. https://doi.org/10.1021/acs.est.1c00515

Zheng YY, Guan HY, Yang J, et al., 2021. Calcium overload and reactive oxygen species accumulation induced by selenium deficiency promote autophagy in swine small intestine. *Anim Nutr*, 7(4):997-1008. https://doi.org/10.1016/j.aninu.2021.05.005